J Mater Sci (2011) 46:2229–2234
DOI 10.1007/s10853-010-5061-8

Thermally evaporated thallium bromide films fabricated at varied substrate temperatures

N. Destefano · M. Mulato

Received: 19 July 2010 / Accepted: 9 November 2010 / Published online: 24 November 2010

Abstract Thallium bromide (TlBr) is a promising semiconductor material for application in room temperature radiation detectors. In this study, the growth of thermally evaporated TlBr films was studied as a function of deposition temperature, from room temperature up to 200 °C. The growth mechanisms were investigated using scanning electron microscopy, energy dispersive spectroscopy, X-ray diffraction, and optical UV–Vis transmittance. The deposition rate drops from 5to 0.8 μm/min, for increasing deposition temperature. Two growth processes were observed and discussed: one where a columnar-like regime dominates and the other where a smaller aspect ratio is obtained with a larger growth in the horizontal direction. This leads to the formation of micrometer-sized crystalline cubes. The variation between growth regimes is temperature dependent. A reduction of the concentration of bromine, discussed based on the vapor pressure values, seems to influence the final structure and optical gap of the samples.

Introduction

Due to its high atomic number, high mass density and intrinsic band gap, thallium bromide (TlBr) has been explored as potential room temperature radiation detector [1, 2]. Most studies related to the fabrication and characterization of TlBr detectors focus on the purification of the original powder and on the growth of bulk crystals [3–8]. Few works have studied polycrystalline TlBr films with large areas ($\sim 40 \times 40$ cm^2), as desired by medical applications [9, 10]. This work investigates the structural, optical, and electrical properties of TlBr films produced by resistive thermal evaporation. This technique presents relative low cost and can be easily expanded for large areas. Furthermore, it has been shown that thermally evaporated TlBr films presented better structural properties and reduced deposition time in comparison with the films produced by spray pyrolysis [11].

The aim of the present article is to contribute for the investigation of the growth mechanisms of TlBr films, to help in optimizing growth conditions for eventual use of such films in X-ray and γ-ray detection applications. In previous works, the evaporation-boat to substrate distance (h) and the number of deposition runs per film (n) were already deeply investigated [12, 13]. The data for the first parameter, h, have shown that larger separations lead to a final material with better structure and morphology, and larger ratios of the photo-to-dark currents, when the system is irradiated under X-ray mammographic energy range [12]. The use of sequential runs (n) is aimed to increase the thickness of the films, as necessary for technological applications. Thicker samples have a larger ratio of the photo-to-dark signal under medical X-ray exposure and a larger linear region as a function of applied voltage [13]. For the experiments described above, all deposition runs were performed keeping the substrates at room temperature. Therefore, this work extends the previous investigation to another fabrication parameter using the thermal evaporation technique: the substrate deposition temperature (T_S). The results are discussed in order to improve even further the properties of the films aimed for medical imagers.

N. Destefano · M. Mulato (✉)
Departamento de Física e Matemática, Faculdade de Filosofia, Ciências e Letras de Ribeirão Preto, Universidade de São Paulo, Av. Bandeirantes 3900, Ribeirão Preto, SP 14040-901, Brazil
e-mail: mmulato@ffclrp.usp.br

Experiments

Thermally evaporated TlBr films were produced on Corning glass 7059 and quartz substrates (1 cm^2). The source to substrate distance was kept at 3 cm, and the boat current was about 58 A, which leads to boat temperatures below 400 °C, according to the previous calibration of the system. The chamber has a total volume of 4 L, and the base pressure before deposition was about 10^{-3} Pa. For each evaporation run 0.25 g of the starting powder (Aldrich 99%) was used. The powder was placed inside a tungsten crucible of about 250 mm^3. This geometry limited the final thickness of the samples for a single run, as presented below. For thicker films, as desired for medical applications, multi-depositions should be used [13]. We studied the influence of substrate temperature (T_S, from room temperature up to 200 °C) on the final properties of the films.

Scanning electron microscope (Zeiss EV050, accelerating voltage of 20 kV) was used to investigate the morphology of either the surface and the cross-section of the samples. Elemental microanalysis was based on energy dispersive spectroscopy (EDS). An IXRF accessory (500 Digital Processing model) was attached to the SEM system for that aim. The EDS peaks of Br and Tl were compared to the respective data of the original starting powder because a standard sample was not available. Thus, only relative variations are presented.

The crystalline structure of the samples was studied by X-ray diffraction experiments, using the Cu anode K_α radiation of a Siemens D5005 equipment (wavelength of 1.5406 Å). The scanning was performed with steps of 0.02 degree per second, using coupled θ–2θ configuration. The optical gap of the samples was inferred from experiments of optical transmittance as a function of wavelength (Beckman Coulter, DU 640 model UV–VIS spectrophotometer).

Results and discussion

The morphology of the samples fabricated at varied substrate temperatures (T_S) was investigated by SEM. The results are presented in Fig. 1. The left and the right sides of the figure correspond to the surface and to the cross-section, respectively. During samples fabrication higher substrate temperatures should increase the surface mobilities of the ad-atoms, leading to a better coverage of the substrate. This is indeed the fact as shown by the comparison between Fig. 1a, b. A more homogeneous coverage of the surface of the substrate is observed when T_S is increased from 50 to 75 °C. Note that both the size and the amount of grooves observed at the surface SEM images are diminished with increasing T_S. The right side of Fig. 1a, b shows the columnar-like growth.

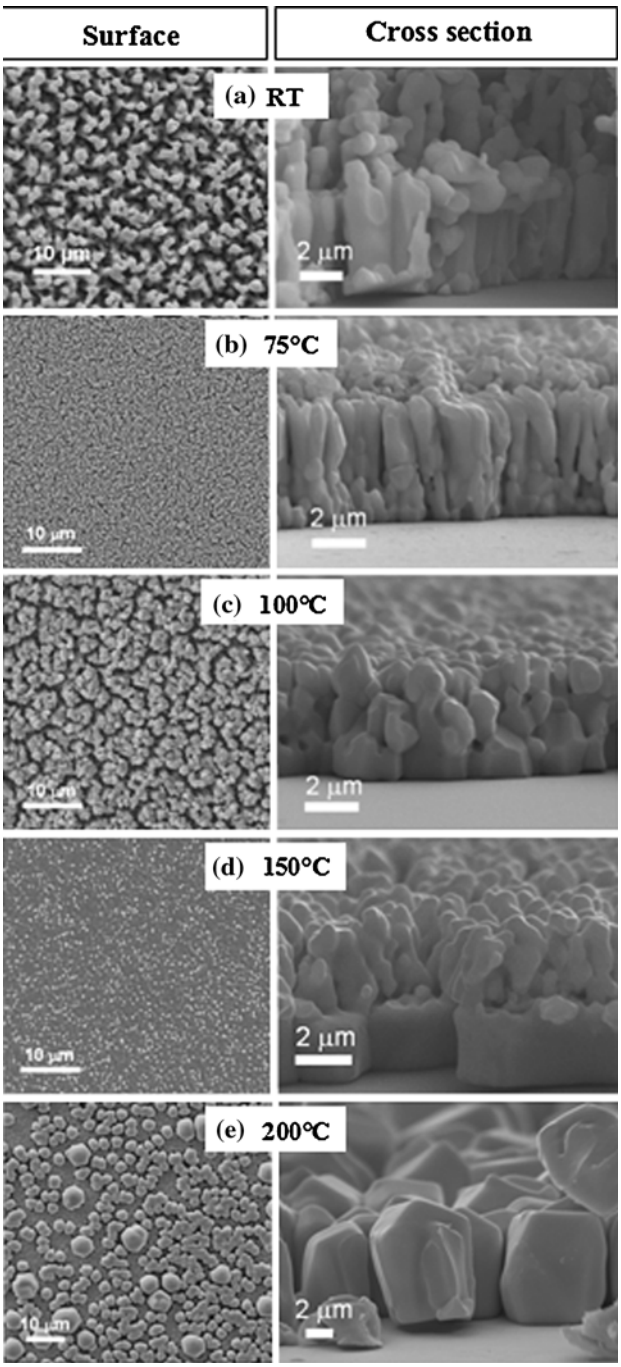

Fig. 1 Scanning electron microscopy images of the surface and the cross-section of the samples for varying substrate deposition temperatures: **a** RT, **b** 75 °C, **c** 100 °C, **d** 150 °C, and **e** 200 °C. Each run was performed using an evaporation-boat to substrate distance of 3 cm, and 0.250 g of the starting thallium bromide powder

For higher substrate temperatures of about 100 °C, a distinct phenomenon is observed. Two distinct growth processes happen subsequently. The first process dominates for regions very close to the substrate, where the temperature is higher. Higher temperatures assure higher

horizontal ad-atom mobilities, leading to the formation of structures with larger horizontal extensions, i.e., smaller aspect ratio. This process dominates for a partial thickness (δ) of about 1.5 μm, as seen in Fig. 1c. The adhesion of additional ad-atoms that will form new layers is determined by the previously discussed columnar growth. Note that this leads to a final surface with worse quality (see Fig. 1c).

The results presented in Fig. 1a–c could have their origin in different physical reasons: (i) once that the growth process occurs at deposition rates of about 1 μm/s, a non-equilibrium process might lead to the formation of varying structures according to the temperature of the substrate, i.e., either growth mechanism would dominate for high or low temperatures; or (ii) higher substrate temperatures would lead to less internal stresses for the first deposited layers. This would cause a smaller amount of crystallographic faults, leading to growth in larger horizontal extensions. In this sense, it would take longer for the influence of eventual stresses to start to dominate and modify the process to the columnar-like regime; or (iii) the deposition rate might not be constant for the whole deposition process. Variations of the deposition rate might lead to varied growth mechanisms.

We believe that the three effects described above might even combine during the fabrication of the samples, but it is not possible at this moment to point out the dominant one. According to the experimental findings, in case T_S is increased above 100 °C, larger values of δ should be found. This is indeed the case as confirmed by the SEM micrographs presented in Fig. 1d and e for T_S equal to 150 and 200 °C, respectively. Note that for $T_S = 200$ °C only one kind of morphology is observed, with the presence of packed micrometer-size crystals. For the case of $T_S = 150$ °C (Fig. 1c) δ increases to about 3 μm, while for $T_S = 200$ °C the corresponding value is about 7 μm.

The total thickness of the samples was calculated using the cross-section SEM micrographs of Fig. 1, and the results are presented in Fig. 2a. An almost constant behavior is observed for T_S equal and above 50 °C. The average value is 4.7 ± 1.5 μm. The only significant variation was observed for the sample fabricated at room temperature, whose thickness is 11.5 ± 2.0 μm. Approximate deposition rates were obtained according to the total thickness and total deposition times. For room temperature, an average deposition rate of about 5.0 μm/min was obtained, while for T_S equal to 200 °C this value was about 0.8 μm/min. For large substrate temperatures the free energy for nucleation is increased, what makes it difficult for the ad-atoms to fix on the sample. As a consequence, part of the evaporated material tends to deposit at other cooled surfaces of the chamber. The deposition rate is in fact the difference between the evaporation rate (material from the boat; ER) and the eventual loss of deposited material due to a re-evaporation (material from the substrate; RR). We observed that longer evaporation times are needed in order to the whole amount of material of the boat be evaporated when the substrate temperature is increased. In this sense, the fact that the thickness remains constant for temperatures above 50 °C as shown in Fig. 2a is just a consequence of the fact that the product (ER − RR) × DT was kept almost constant for all the runs. The deposition of material at cool surfaces of the chamber can be seen at the photographs presented in Fig. 3. The photo at Fig. 3a was taken after a deposition at 200 °C. The whitish regions correspond to material deposited at the bottom of the chamber instead of at the substrates. The extreme case is reached when nothing is deposited on top of the substrate. This is illustrated by Fig. 3b, which corresponds to a deposition performed at 50 °C, and using a higher evaporation-boat to substrate distance of about 9 cm. Note that the evaporated material is also deposited at the walls of the chamber, with a shape that is determined by the temperature distribution.

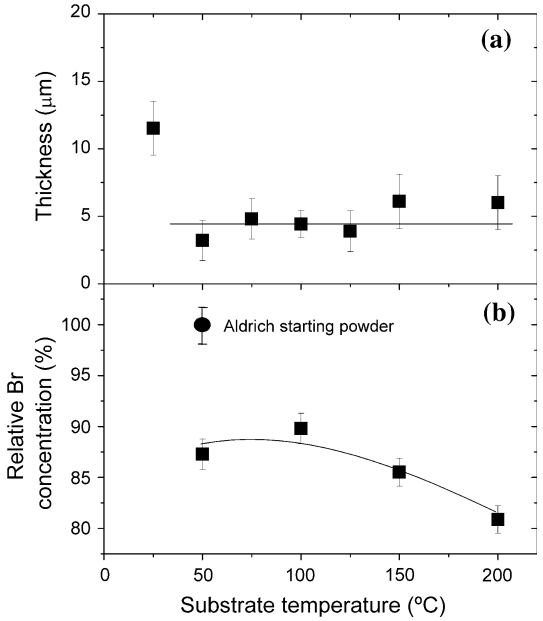

Fig. 2 Total thickness of the samples (**a**) and percentage of bromine atoms (**b**) as a function of substrate deposition temperature. The thickness values were calculated using the cross-section SEM micrographs. The percentage of Br atoms of the initial Aldrich powder is indicated as a *circle* in (**b**) at a fictitious temperature of 50 °C for comparison

The final composition of the samples is also determined by the fabrication temperature. Figure 2b shows the relative percentage of bromine () atoms as a function of T_S. The value of the initial Aldrich powder is used as reference (indicated as 100% in Fig. 2b at a temperature of 50 °C for comparison). In the same figure, the data for the fabricated samples are presented as squares. The amount of bromine

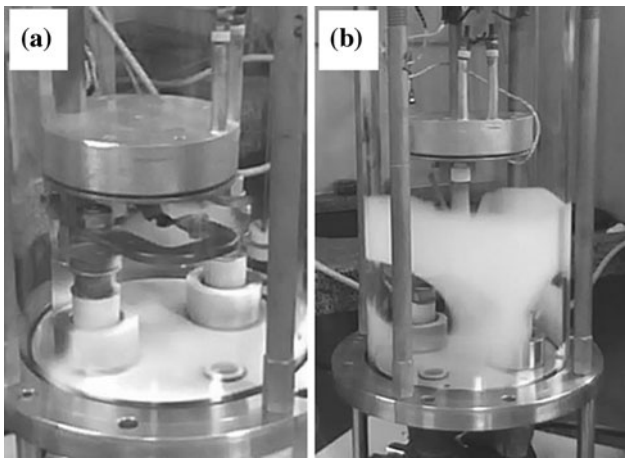

Fig. 3 Photography of the deposition chamber after a run performed using **a** an evaporation-boat to substrate distance of 3 cm and $T_S = 200$ °C and **b** an evaporation-boat to substrate distance of 9 cm and $T_S = 50$ °C. The *whitish regions* in both correspond to material deposited at the bottom and at the walls of the chamber, with a shape that is determined by the temperature distribution

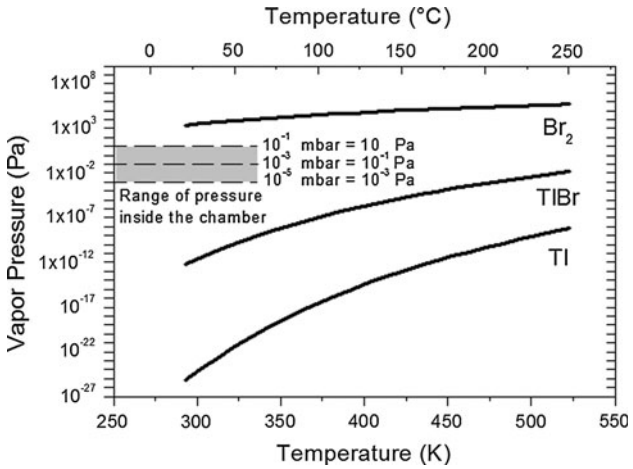

Fig. 4 Vapor pressure curves for bromine (Br_2), thallium bromide (TlBr), and thallium (Tl) as a function of temperature. The values were extrapolated according to the equations and suggested numerical coefficients presented at the literature [14]. The expected pressure range inside the chamber during the whole process is also illustrated as a *light gray rectangle*

decreases with increasing T_S. As already discussed elsewhere [12, 14], bromine and thallium have very different vapor pressure (VP) values. The variation of VP with temperature is reproduced in Fig. 4, where the values were extrapolated according to the equations and suggested numerical coefficients presented in the literature [14]. From top to bottom the corresponding curves for bromine (Br_2), TlBr, and thallium (Tl) are presented. At the left side of the figure, the expected range of pressure inside the chamber during the whole process is illustrated. The base pressure before evaporation would be about 10^{-3} Pa, and the pressure during film growth might achieve 10 Pa. Note, however, that the VP value for thallium is always smaller than any value of this range. The opposite happens for bromine.

During evaporation the temperature of the boat can vary from ambient to above 1,000 °C. Several species can leave the boat such as Tl, Br, and TlBr. They all are directed toward the substrate that sits at a much smaller temperature. The ad-atoms form a growing film. In this sense, the data in Fig. 4 can help to understand the relative variation of Br in the final samples. The fact that VP for bromine is above the pressure inside the chamber, and that it increases with temperature explains the observed bromine reduction in Fig. 2b. Larger VPs make more difficult the adhesion of Br atoms on top of the substrates due to a re-evaporation process.

TlBr has a cubic crystal structure of a CsCl type, a melting point close to 480 °C, and no destructive phase transition between room temperature and melting point [15]. Taking that into account, the XRD patterns of the samples of the present work are presented in Fig. 5, from

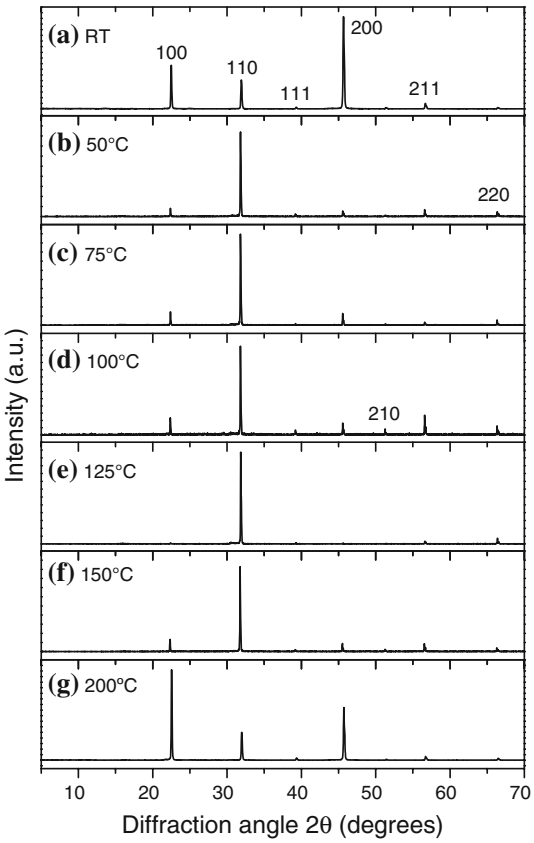

Fig. 5 XRD spectra for varying substrate deposition temperatures from room temperature (RT) up to 200 °C. Each run was performed using an evaporation-boat to substrate distance of 3 cm, and 0.250 g of the starting thallium bromide powder. With increasing deposition temperature the most intense peak is observed at smaller diffraction angles

top to bottom for increasing substrate deposition temperatures. For room temperature the most intense peak is the (200), but other diffraction peaks are also observed. For temperatures from 50 up to 150 °C the most intense is the 110. Note that this is correlated with the variation of the morphology, as presented from Fig. 1a–d. No great variations in the diffractograms are observed because the diffraction comes from the topmost regions of the sample while the main morphological and crystallographic variations are occurring at the bottommost regions. Above 150 °C, the most intense diffraction peak is the (100). Note the correlation with the strong morphological variation from Fig. 1d, e, where only one growth mechanism dominates for the last case. Thus, for increasing deposition temperature, and decreasing Br content as already discussed, the most intense peak is observed at smaller diffraction angles. The change of the dominant growth phenomenon leads to the observed variations of morphology and crystallographic orientations. It should be pointed out that for a different starting powder (Merck, 99.9%), and the same deposition conditions at room temperature, the most intense peak is the (100). For that case, the starting powder has a smaller Br content then in the present case [13]. It confirms that both deposition rate and stoichiometry determine the final structure.

The integrated area of each diffraction peak was used for a deep study of the relative crystallinity of the samples. A_{110}, A_{100}, and A_{200} correspond to the integrated areas of peaks (110), (100), and (200), respectively. The total area for the whole spectrum is represented as A_{hkl}. Figure 6a shows the A_{110} to A_{hkl} ratio as a function of substrate deposition temperature. A drastic decrease is only observed for T_S equal to 200 °C. This might suggest that no variation exists for substrate temperatures from 50 up to 150 °C. This is not the case as evidenced by the data in Fig. 6b. In this figure, A_{110} to either A_{100} or A_{200} ratios are presented, respectively, as squares and circles. Both ratios decrease with increasing T_S. This suggests that (i) the presence of other less important diffraction peaks is reduced; and (ii) the (100) and (200) peaks become more relevant for higher deposition temperatures. These variations are due to many physical facts such as surface ad-atom mobility variation, deposition rate variation, and reduction of Br atoms with temperature.

The optical properties of the films were also investigated. Figure 7 shows the transmittance as a function of wavelength for the sample fabricated at T_S equal to 150 °C. Total absorption is observed below 421 nm, and the maximum transmittance is about 15%. The same qualitative behavior is observed for samples fabricated at other T_S values. The only difference was observed for the film fabricated at $T_S = 200$ °C due to the non-zero transmittance for low wavelengths. The regions between the

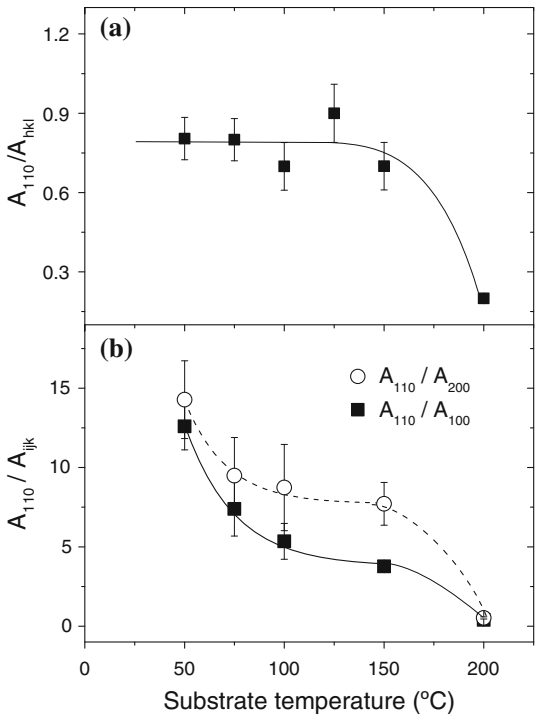

Fig. 6 **a** Normalized integrated area of the 110 X-ray diffraction peak as a function of substrate deposition temperature (T_S) for each run. **b** Ratio of the integrated area of the 110 to the 100 peak (*dark squares*) and to the 200 peak (*white circles*) as a function of T_S

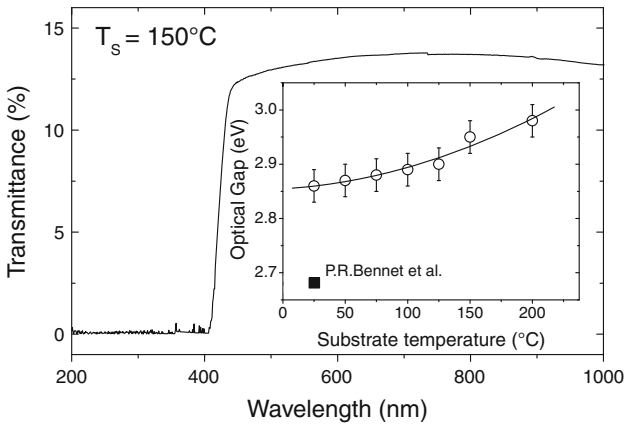

Fig. 7 Optical UV–Vis transmittance as a function of wavelength for the film produced at $T_S = 150$ °C. The *inset* shows the increase of the optical gap with varying substrate deposition temperature as *circles*. The *solid square* of the *inset* corresponds to data extracted from the literature for comparison [10]

disperse grains (see Fig. 1e) might allow the passage of light without absorption in this case. The optical gap (E_g) was calculated using the derivative method [16]. The calculated values are presented in the inset of Fig. 7. As already previously reported [12, 13] the values of optical gap obtained for our samples are always larger than the literature. A value extracted from the literature is also presented for comparison [10]. Note the monotonic

increase of E_g with increasing deposition temperature. We believe that this is associated to the variation of structure and total amount of Br atoms in the samples.

Conclusions

TlBr evaporated films were studied as a function of deposition temperature. Higher substrate temperatures lead to larger surface mobility of the ad-atoms, with a better coverage of the substrate. Two growth regimes were observed for varied deposition temperatures. The first regime, that leads to a columnar-like structure, dominates for temperatures below 100 °C. Above this temperature the second regime dominates for regions very close to the substrate, leading to the formation of structures with larger horizontal extensions, i.e. smaller aspect ratio. A packing of micrometer-sized crystals are obtained in this case for $T_S = 200$ °C. The growth regimes are determined by a possible combination of temperature gradient, stresses or rate variation. The concentration of bromine is reduced with increasing deposition temperature. This is determined by the difference in VP of the evaporated elements, combined with the temperature distribution inside the chamber. For increasing deposition temperature, and decreasing Br content, the most intense X-ray diffraction peak is observed at smaller diffraction angles. It confirms that both deposition rate and stoichiometry determine the final structure. The values of optical gap obtained for our samples are always larger than presented in the literature. A monotonic increase with increasing deposition temperature was measured. We believe that this is associated to the variation of the structure and total amount of Br atoms in the samples. The purity of the starting material was 99%, which prevents any electrical characterization of the final samples. The optimized conditions to produce X-ray detectors in the future would be: (i) the use of more purified starting material; (ii) a deposition temperature close to 200 °C, (iii) the use of heated chamber walls, (iv) an atmosphere with excess Br atoms to compensate the stoichiometry of the final film, and (v) the control of morphology and grain geometry to match the required size of the detectors voxels using the sandwich configuration of electric contacts.

Acknowledgements This work was funded by FAPESP, CAPES, and CNPq. The authors thank J. L. Aziani, M. Mano Jr, E. A. Navas, and S.O.B. da Silva for experimental help.

References

1. Sellin PJ (2006) Nucl Instrum Methods Phys Res A 563:1
2. Ponpon JP (2005) Nucl Instrum Methods Phys Res A 551:15
3. Onodera T, Hitomi K, Shoji T, Hiratate Y (2004) Nucl Instrum Methods Phys Res A 525:199
4. Owens A, Bavdaz M, Brammertz G, Gostilo V, Haack N, Kozorezov A, Lisjutin I, Peacock A, Zatoloka S (2003) Nucl Instrum Methods Phys Res A 497:359
5. Kouznetsova MS, Lisitskya IS, Zatolokab SI, Gostilo V (2004) Nucl Instrum Methods Phys Res A 531:174
6. Kozlov V, Leskela M, Sipila H (2005) Nucl Instrum Methods Phys Res A 546:200
7. Kozlov V, Leskela M, Prohaska T, Schultheis G, Stingeder G, Sipila H (2004) Nucl Instrum Methods Phys Res A 531:165
8. Hitomi K, Matsumoto M, Muroi O, Shoji T, Hiratate Y (2001) J Cryst Growth 225:129
9. Olshner F, Shah KS, Lund JC, Zhang J, Daley K, Medrick S, Squillante MR (1992) Nucl Instrum Methods Phys Res A 322: 504
10. Bennett PR, Shah KS, Cirignano LJ, Klugerman MB, Moy LP, Olschner F, Squillante MR (1999) IEEE Trans Nucl Sci 46:266
11. Destefano N, Mulato M (2009) In: MRS symposium proceedings, vol 1164, p L09-11
12. Destefano N, Mulato M (2009) Master thesis. University of São Paulo-USP, Brazil
13. Destefano N, Mulato M (2010) Nucl Instrum Methods Phys Res A 624:114
14. Yaws CL (1995) Handbook of vapor pressure, vol 4. Gulf Publishing Company, Houston
15. Hitomi K, Muroi O, Matsumoto M, Hirabuki R, Shoji T, Suehiro T, Hiratate Y (2001) Nucl Instrum Methods Phys Res A 458:365
16. Silva AF, Veissid N, An CY, Pepe I, Oliveira NB, da Silva AVB (1996) Appl Phys Lett 69:1930